American Mineralogist, Volume 76, pages 602–610, 1991

Determination of the nonequilibrium ordering state in epidote from the ancient geothermal field of Saint Martin: Application of Mössbauer spectroscopy

PATRICIA PATRIER, DANIEL BEAUFORT, ALAIN MEUNIER

Laboratoire de Pétrologie des Altérations Hydrothermales, Université de Poitiers, U.A. 721 C.N.R.S., 40, Avenue du Recteur Pineau, Poitiers Cédex 86022, France

JEAN-PAUL EYMERY

Laboratoire de Métallurgie Physique, Université de Poitiers, U.A. 131 C.N.R.S., 40, Avenue du Recteur Pineau, Poitiers Cédex 86022, France

SABINE PETIT

Laboratoire de Pétrologie de la Surface, Université de Poitiers, U.A. 721 C.N.R.S., 40, Avenue du Recteur Pineau, Poitiers Cédex 86022, France

ABSTRACT

The island of Saint Martin (Lesser Antilles) offers a lateral cross section of the roots of a porphyry deposit system. In the several-kilometer alteration halo developed around the intrusion, epidote is commonly observed. This mineral exhibits a great diversity in chemical composition. In the absence of associated hematite, the Fe content, as well as the chemical dispersion, increase with the distance from the intrusion. For a better understanding of epidote intrasample chemical variations, Mössbauer spectra have been obtained from five samples. Fe^{3+} ions accommodated in M3 sites represent the majority of the total Fe present ($\geq$90%), but significant amounts assigned to M1 sites have been measured. An increase of epidote disorder with increased distance from the intrusion has been demonstrated. A good correlation is observed between the deviation from the equilibrium ordering state of epidotes and paleotemperature distribution. Rapid crystallization cannot explain this disequilibrium state because nonisothermal diffusion or interface controlled growth decreases the epidote crystallization rate with distance from the thermal source. Our observations suggest that epidotes formed near the intrusive body, at temperatures above 300 °C, display an equilibrium state of order-disorder. Away from the intrusive body the nonequilibrium ordering state of epidote increases with distance from the intrusion and is preserved because of the low temperature and low diffusion rates.

INTRODUCTION

Epidote [$Ca_2Al_2(Al,Fe)Si_3O_{12}OH$] is a common rock-forming mineral found in geothermal fields and low-grade metamorphic environments. This mineral develops complex zoning and may exhibit great diversity in chemical composition. Many studies have investigated the factors controlling the chemical composition of epidote. From the numerous petrological observations and thermodynamical calculations, epidote has been found to vary in chemical composition as a function of bulk composition, temperature, pressure, pH and CO_2, S_2, and O_2 fugacities (Bird et al., 1988; Caruso et al., 1988; Grapes and Watanabe, 1984; Hietanen, 1974; Liou, 1973; Miyashiro and Seki, 1958; Raith, 1976; Shikazono, 1984).

As the distribution of Fe^{2+}-Fe^{3+} ions in the crystal lattice is obtainable by Mössbauer spectrometry, the substitutional order-disorder in epidote can be calculated. This parameter provides information concerning the stable-metastable state of epidote.

Mössbauer spectra of epidotes have been previously reported by Bancroft et al. (1967), Coey (1984), De Coster et al. (1963), Dollase (1973) and Paesano et al. (1983). These authors studied synthesized or natural (including heat-treated) products from diverse geologic occurrences and focused their works strictly on Fe site assignments. Bird et al. (1988) were the first to use this spectroscopy for samples from a single geological environment (Salton Sea geothermal field) in order to determine the extent to which metastable composition occurs in epidote. However, their results are restricted by the small number of samples studied.

The lateral cross section of Saint Martin (Lesser Antilles) is of great interest in the sense that it displays the roots of a porphyry deposit system. Previous studies have investigated the lateral distribution of alteration (Beaufort et al., 1990) and the epidote morphological and compositional variations (Patrier et al., 1990; Beaufort et al., in preparation).

Our work focuses on ^{57}Fe Mössbauer spectroscopy of epidote from this ancient geothermal field. The objectives

0003–004X/91/0304–0602$02.00

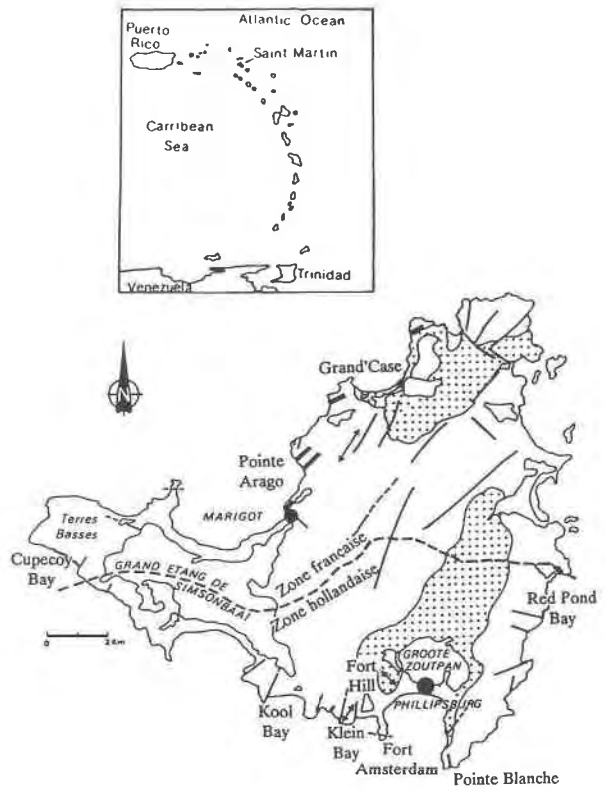

Fig. 1. Geological map of Saint Martin. The dotted area represents the quartz-diorite pluton (Beaufort et al., 1990).

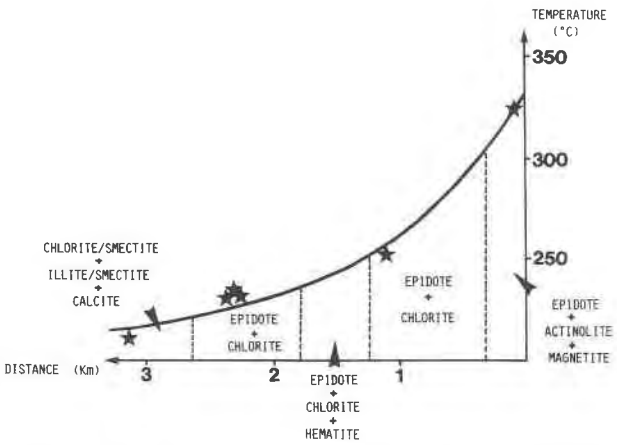

Fig. 2. Paleotemperatures profile, measured from quartz fluid inclusions (stars) in veins bearing quartz + epidote, and pervasive alteration pattern developed around the intrusive complex of Saint Martin (Beaufort et al., 1990). Temperatures are estimated from the first generation of fluid inclusions observed in propylitic and argillic veinlets.

are first to determine the order-disorder degree by the distribution of Fe^{3+} ions between M1 and M3 sites and second to relate the extent of the metastable composition of epidote to location. The nonequilibrium ordering state, deduced from the model of Bird and Helgeson (1980), will be discussed in terms of paleotemperature profile.

Geological background

Field setting

The island of Saint Martin belongs to the volcanic arc of the Lesser Antilles and is located in the west-central portion of Anguilla Bank (northeast Lesser Antilles). This region consists of alternating sedimentary and andesitic to dacitic volcaniclastic rocks (from Eocene epoch) intruded by a quartz-diorite complex of Oligocene age (Fig. 1). Important geothermal activity accompanied the emplacement of the intrusive complex and produced a several-kilometer wide alteration halo. The geology of this fossil geothermal system, as well as the lateral distribution of alteration, have been described by Beaufort et al. (1990).

The stratigraphy consists of a lower sequence of alternating marls and limestones, a medium sequence of hyaloclastites and lava flows intercalated with cherty layers, and an upper sequence of hyaloclastites and tuffs. At the contact of the pluton, host rocks have been recrystallized into hornfels (200–300 m thick).

At present, the island displays a continuous lateral cross section of the roots of the hydrothermal system, from the intrusive body to the more external parts.

In zones of high fracture permeabilities (regional and magmatic fractures), the observed alteration sequence consists of progressive fractures filled with minerals of the potassic (tourmaline + quartz + magnetite + orthoclase + apatite + sulfides), then phyllic (phengite + quartz ± pyrite), and then sometimes argillic (dickite + quartz) facies. On the basis of a fluid inclusion study (Beaufort et al., 1990), this sequence has been interpreted to be the result of progressive dilution of early magmatic brines.

Zones of low fracture permeability represent the major part of the geothermal system. They display a regular alteration zoning (Fig. 2): (1) epidote + quartz-bearing assemblage (propylitic alteration) up to 3 km from the pluton and (2) mixed-layer minerals + calcite assemblage (intermediate argillic alteration) that extends one kilometer outward.

The study of primary fluid inclusions of quartz, associated with epidote, and of calcite, associated with mixed-layer minerals indicates that this alteration zoning, emplaced in environments of inactive flow regime, was mainly controlled by the thermal diffusion gradient (140–350 °C) generated by the pluton.

Phase relations in assemblages including epidote

The epidote-bearing paragenesis is observed continuously as far as 3 km from the intrusion. It occurs as replacement of the groundmass and as veinlet fillings. Epidote crystallized in three distinctive secondary assemblages (Fig. 2). (1) An epidote + actinolite + quartz ± magnetite assemblage restricted near the intrusion (0–

Table 1. Samples investigated for Mössbauer spectroscopy

	Samples			
	SM4	SM17 (≈ SM14)	SM112	SM43
Rock type	hyaloclastite	fine grained hyaloclastite	hyaloclastite	miarolitic vugs in the quartz diorite
Distance from the intrusion	≈2.5 km	≈2.1 km	≈1.6 km	
Temperature (*T*)	≈225 °C	≈233 °C	≈277 °C	≈340 °C
Alteration paragenesis	EP + CHL + QZ superimposed by low *T* event		EP + CHL + QZ + HM	EP + ACT + QZ ± MG (pervasive alteration)

Note: Paleotemperatures are provided by quartz fluid inclusion data (Beaufort et al, 1990). Abbreviations: EP = epidote, QZ = quartz, CHL = chlorite, HM = hematite; ACT = actinolite, MG = magnetite.

300 m from the pluton). The associated temperature covers 300–350 °C. (2) An epidote + chlorite + quartz assemblage that replaces, up to 3 km from the intrusion's side, the hyaloclastite sequence for temperatures ranging from 220 to 300 °C. (3) An epidote + chlorite + hematite + quartz assemblage that represents the alteration of Fe- and Mn-rich cherty layers located approximately 1.5 km from the intrusion.

Fluid salinities vary from 30 wt% NaCl-eq. (in actinote zone) to 3 wt% NaCl-eq. at 3.3 km from the pluton.

The temperature range for epidote crystallization (225–350 °C) is in good agreement with the thermal stability fields reported in geothermal systems (Bettison and Schiffman, 1988; Bird et al., 1984; Cavaretta et al., 1985; Shikazono, 1984).

Experimental methods

Chemical composition

Epidotes were analyzed on polished thin sections using a Cameca MS 46 electron microprobe equipped with an Ortec energy dispersive X-ray analyzer. The accelerating voltage and the sample current were, respectively, 15 kV and 1.5 nA. The counting time was 100 s.

In order to assess chemical zoning, analyses were obtained with a spot size of 1 μm on a SX50 Cameca microprobe equipped with wavelength dispersive spectrometers. The counting time was 10 s for each element. These systems were calibrated with synthetic or natural oxides and silicates. Corrections were made with a ZAF computing program. The reproductibility of standard analyses was 1% for each element routinely analyzed.

X-ray diffraction

X-ray diffractograms of randomly oriented powder were performed on a Philips PW1730 diffractometer (Co anode, 40 kV, 40 mA).

Mössbauer spectrometry

Mineral separates. On the basis of the previous studies, five samples were selected. Four samples belong to the hyaloclastite sequence (SM4, SM14, SM17, and SM112) and one belongs to the miarolitic vugs developed in the intrusion (SM43) (Table 1).

The samples were extracted from veins bearing epidote + quartz, which are sometimes crosscut by calcite, (samples SM17, SM112, and SM14) and from miarolitic vugs (sample SM43) with a drilling needle. For sample SM4, the most highly altered parts of the rock (epidote + quartz paragenesis superimposed by low temperature event) were finely ground. Because they were closely associated, epidote and quartz were difficult to separate, even by magnetic methods. The mineralogical compositions of the concentrates were determined by X-ray diffraction. Concentrates obtained from sample SM43 were monomineralic. In addition to epidote, the other concentrates contained the following minor impurities: (1) minor quartz (samples SM14–SM112), (2) minor quartz and calcite (sample SM4), and (3) minor quartz and traces of white micas (sample SM17). No other Fe-bearing minerals were detected in these impurities.

Instrumentation. All spectra were obtained from finely ground powders at room temperature. They were obtained on an Elscint A.M.E.30 spectrometer (Métallurgie Physique laboratory, Poitiers University). A ^{57}Co in Rh source of nominal activity 25 mCi was used. Signals were recorded on a multichannel analyzer. Isomer shifts were calculated vs. Fe metal. Deconvolutions, based on least-squares fitting procedures, assumed Lorentzian line shapes. Each absorption doublet was characterized by the isomer shift, quadrupole splitting, peak intensity, and line width.

Epidote compositional and morphological variations

The epidote group minerals from Saint Martin are slightly inhomogeneous with regard to their Fe^{3+}/Al^{3+} ratio.

Microprobe analyses taken across crystal grains show two types of chemical zonings. These consist essentially of various diffusion zonings (some grains develop Fe-rich cores, whereas others are characterized by Fe-rich rims), and periodic chemical oscillations between approximately $X_{Ps} = 0.15$ and $X_{Ps} = 0.25$ as observed in sample SM43. Despite these, average values evidenced some chemical trends.

The percentage of pure Fe + Mn end-member [i.e., $Ca_2(Fe, Mn)_3Si_3O_{12}(OH)$] expressed by the ratio $Fe^{3+} + Mn^{3+}/Fe^{3+} + Mn^{3+} + Al^{3+}$, increases with distance from the intrusion. However, the maximum average value (33%) is found for epidote in replacement of oxidized

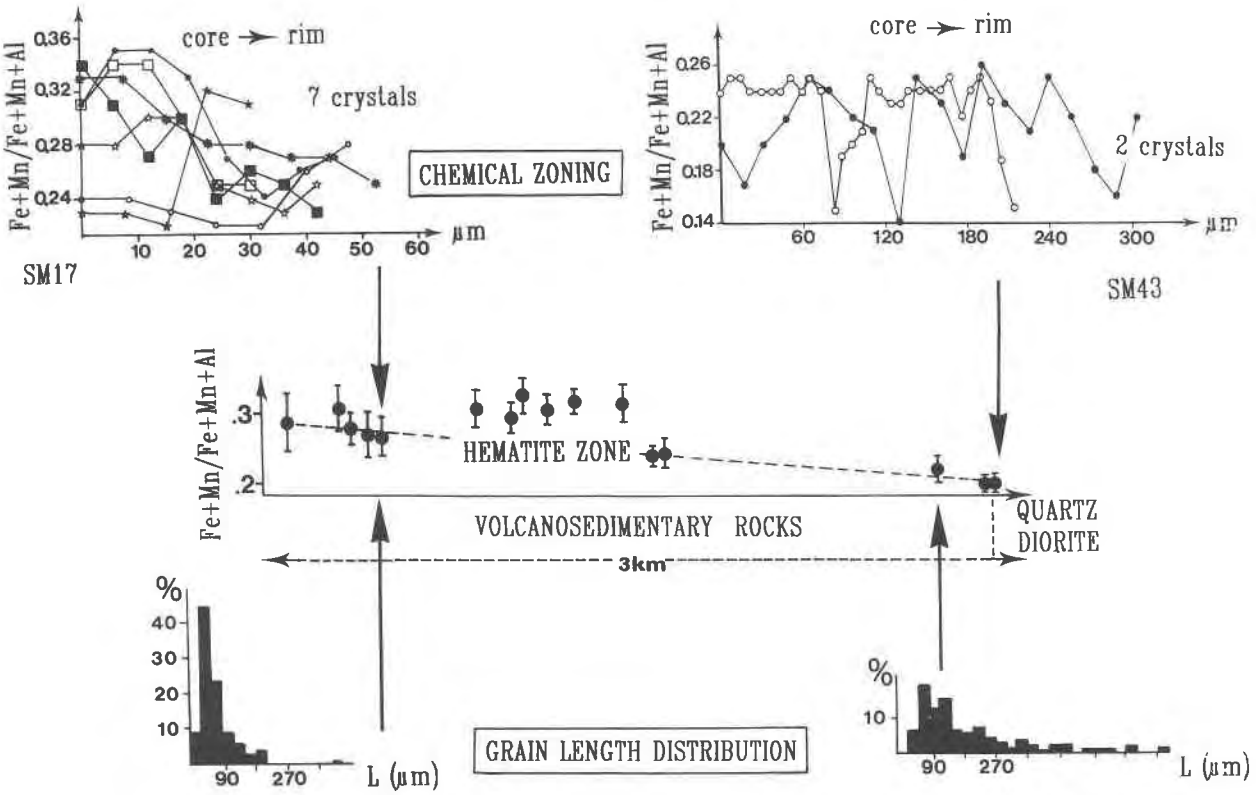

Fig. 3. Chemical composition of epidote samples as well as their compositional variations, expressed by Fe + Mn/Fe + Mn + Al atomic ratio (average values and standard deviations), plotted in terms of distance from the quartz-diorite pluton. In the hematite zone, where the epidote + chlorite + hematite paragenesis is encountered (i.e., in Fe cherts), the X_{Ps} ratio is close to 0.33.

Two main types of zoning of epidotes (expressed by Fe + Mn/Fe + Mn + Al ratio) have been observed. Oscillatory chemical variations can be observed in epidotes from miarolitic vugs, whereas the epidote sampled well away from the pluton displays irregular zoning. The grain length (L) distribution is expressed in percentage of grains. These histograms have been determined from more than 100 grains (Patrier et al., 1990).

lithologic formations (Fe-rich cherts) where the propylitic paragenesis contains hematite. Except in the hematite zone, no correlation was obtained between the Fe_2O_3 content of host rock and the Fe_2O_3 content of epidote. For the samples studied (chemical compositions listed in Table 2), the average X_{Ps} ratio ranges from 0.20 to 0.29.

Mn-rich epidotes crystallized in Mn-rich Fe cherts (up to 2.45% Mn_2O_3). However, in samples available for Mössbauer spectroscopy, Mn content does not exceed 0.03 atom per formula unit.

The difference between maximum and minimum Fe content for each sample is approximately constant. However, intrasample chemical variations, obtained from average values and standard deviations calculated from microprobe analyses (Table 2), increase with distance from the intrusion. The atomic ratio Fe^{3+} + Mn^{3+}/Fe^{3+} + Mn^{3+} + Al^{3+}, in sample SM4, ranges from 0.24–0.33, whereas, in the hornfels halo, it is 0.20 to 0.22.

Epidote crystallized in a euhedral habit only in veins. In the groundmass, the host minerals prevent coarsening of euhedral habits. From a previous grain-size study of epidote crystallizing in veins (Patrier et al., 1990), it appeared that epidote sizes were highly influenced by temperature distribution; the lengths and widths decreased exponentially with distance from the intrusion.

All of these observations have been generalized in Figure 3.

Results

Mössbauer spectroscopy

Epidote can be represented by the formula $A_2M_3Si_3O_{13}H$. According to Dollase (1971), its structure contains two types of chains, a single chain of edge sharing M2 octahedra and a multiple chain of central M1 and peripheral M3 octahedra attached on alternate sides. These chains are cross linked by SiO_4 tetrahedra and Si_2O_7 groups which share some of their O atoms. The large cavities developed in this framework contain nine- or ten-coordinated Ca cations.

Although there is a wide variation in Fe^{3+}-Al^{3+} distribution, no significant substitutions occur in the tetrahe-

Table 2. Electron microprobe analyses of epidote used for Mössbauer spectroscopy

	Samples				
	SM4	SM14	SM17	SM112	SM43
Si	5.96 ± 0.10	6.03 ± 0.07	5.97 ± 0.05	6.06 ± 0.03	5.97 ± 0.05
Al	4.34 ± 0.23	4.34 ± 0.20	4.50 ± 0.17	4.42 ± 0.17	4.75 ± 0.07
Fe^{3+}	1.74 ± 0.27	1.62 ± 0.23	1.53 ± 0.16	1.54 ± 0.16	1.16 ± 0.08
Mg	0.02			0.01	0.03
Ti				0.01	0.01
Mn^{3+}	0.02	0.01	0.04	0.04	0.06
Ca	3.93 ± 0.04	3.99 ± 0.07	3.97 ± 0.07	3.90 ± 0.04	4.05 ± 0.12
X_{Ps}	0.29	0.27	0.25	0.26	0.20
N	30	27	29	34	31
SiO_2	37.52	38.06	37.19	38.08	37.63
Al_2O_3	23.18	23.92	23.77	23.62	25.40
Fe_2O_3	14.55	13.09	12.64	12.89	9.74
MgO	0.07			0.03	0.15
TiO_2				0.08	0.10
Mn_2O_3	0.14	0.13	0.35	0.31	0.49
CaO	23.08	23.31	23.08	22.95	23.83
TOTAL	98.54	98.51	97.03	97.97	97.34

Note: Structural formulae are based on 25 O atoms. Total Fe is expressed as Fe_2O_3. X_{Ps} = Fe/Fe + Al atomic ratio. N = number of analyses.

dral sites, and substitutions for Ca^{2+} by Fe^{2+}, Mn^{2+}, Mg^{2+} do not exceed 0.1 atom per formula unit (Deer et al., 1962).

Dollase (1971) showed that M2 sites accomodate only Al^{3+} and that M3 sites contain a larger fraction of Fe^{3+} (and Mn^{3+}) compared to the smaller M1 sites. For epidotes having 0.8–1 Fe^{3+} per formula unit, no more than 14% of the total Fe^{3+} is located in the M1 site. Mössbauer spectra (Bancroft et al., 1967; Coey, 1984; De Coster et al., 1963) confirm that Fe^{3+} is preferentially distributed in the asymmetric M3 site.

Mössbauer spectra of the selected samples are depicted in Figure 4. Their respective Mössbauer parameters are listed in Table 3. One absorption doublet is observed for sample SM43. This doublet is characterized by an isomer shift (δ) close to 0.36 mm/s and by a large quadrupole splitting ($\Delta \approx 2.06$ mm/s). Considering the isomer shift value, this signal is unambiguously attributed to Fe^{3+}. These results match the Mössbauer data reported by Bancroft et al. (1967), Coey (1984), De Coster et al. (1963), and Dollase (1973). The large value of quadrupole splitting is consistent with Fe^{3+} located in the largest and more distorted M3 site. The line width (Γ), close to 0.35 mm/s, is in agreement with previous works (Dollase, 1973; Paesano et al., 1983). Bancroft et al. (1967) found a higher value ($\Gamma \approx 0.44$ mm/s); however, according to Dollase (1973), this can be explained by a nonrecognition of a second doublet attributed to Fe^{3+} in the M1 site. This doublet is displayed by all the samples studied ($1.94 \leq \Delta \leq 2.06$; $\delta \approx 0.35$–0.36 mm/s).

In samples SM4, SM14, SM17, and SM112, a second doublet is expressed by an inner shoulder on the prominent doublet. It is particularly well developed in sample SM4. This inner doublet is characterized by an isomer shift close to 0.35 mm/s ($0.31 \leq \delta \leq 0.36$) and by a quadrupole splitting ranging from 0.8 to 1.00 mm/s. The isomer shift values are consistent with Fe^{3+} ions in an octahedral site. Mössbauer spectra confirm that Fe^{3+} ions represent the great majority of the total Fe present. Because of its lower quadrupole splitting, the inner doublet is assigned to Fe^{3+} located in the smallest and more regular M(1) site. Dollase (1973) first described signals attributed to Fe^{3+} in M1 sites. The Mössbauer parameters, provided by this study, are slightly different from those observed by this author. However, the inner shoulder, well developed on the major doublet, allows an accurate estimation of δ and Δ values. The values of quadrupole splitting are similar to those described by Dollase (1973) for piedmontite, $Ca_2(Mn,Fe,Al)_3OOH[Si_2O_7][SiO_4]$; however, in all the epidotes analyzed, Mn content does not exceed 0.03 atom per formula unit.

The inner doublet is better developed with higher Fe

Table 3. Parameters of Mössbauer spectra for epidote from the ancient geothermal field of Saint Martin

	Samples					
	4a	4b	14	17	112	43
	Fe^{3+} in M3					
Width Γ (mm/s)	0.33	0.35	0.31	0.35	0.34	0.35
Isomer shift δ (mm/s)	0.36	0.36	0.36	0.35	0.36	0.36
Quadrupole splitting Δ (mm/s)	2.00	2.00	2.00	1.94	1.99	2.06
Area	0.90	0.86	0.92	0.91	0.95	1.00
	Fe^{3+} in M1					
Width Γ (mm/s)	0.40	0.40	0.50	0.40	0.40	
Isomer shift δ (mm/s)	0.34	0.31	0.36	0.35	0.34	
Quadrupole splitting Δ (mm/s)	0.80	0.90	1.00	0.90	0.90	
Area	0.10	0.11	0.08	0.09	0.05	
		Fe^{2+}				
Width Γ (mm/s)		0.34				
Isomer shift δ (mm/s)		1.11				
Quadrupole splitting Δ (mm/s)		1.80				
Area		0.03				

Note: Isomer shift values are relative to metallic Fe. Standard deviation for area is ±3%. For sample SM4, two groups of values were obtained from best fitted deconvolutions, one with and one without a Fe^{2+} Doublet.

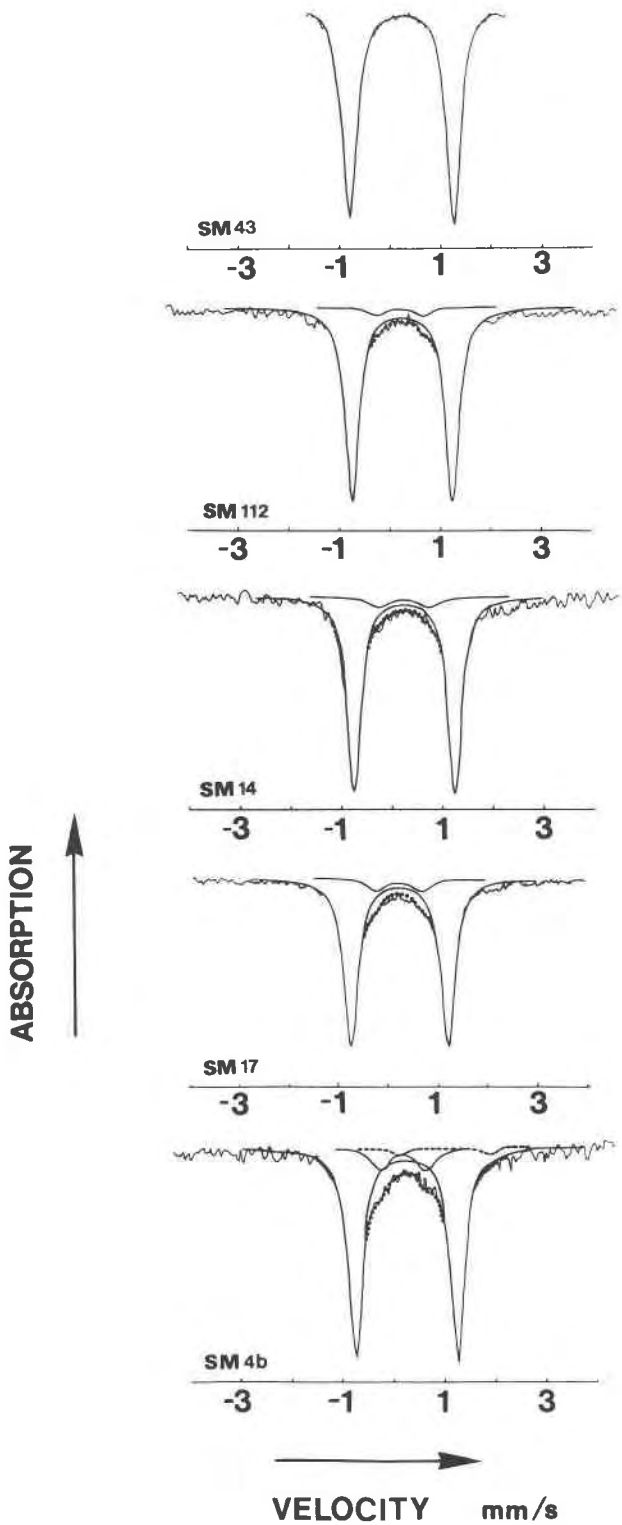

Fig. 4. Mössbauer spectra of the epidotes studied. Solid curves = doublets attributed to Fe^{3+} in M3 and M1 sites. Dashed curves = doublet attributed to Fe^{2+}. Circles = calculated fit. For sample SM4, only the best fitted deconvolution, taking the Fe^{2+} signal into account, is depicted (sample 4b).

content. The maximum Fe^{3+} content accommodated in the M1 site (10–11% of total Fe) is observed in sample SM4. Samples SM14 and SM17 exhibit only slightly lower content with the same peak widths: 9% of the total Fe. The maximum value given by Dollase (i.e., 14%) is attributed to more Fe-rich epidote samples, i.e., epidote samples synthesized with hematite buffers (X_{Ps} close to 0.33). Because the achievement of the best fit produces greater peak widths for low Fe content, these widths have been constrained to values close to 0.4 mm/s ($0.4 \leq \Gamma \leq 0.5$), i.e., values displayed by the SM4 spectra. Introducing the doublet for Fe in M1 for the deconvolution of the spectrum obtained for sample SM43 does not improve the fit.

In sample SM4, the least-squares fitting procedure gives best results when a third doublet, characterized by a quadrupole splitting close to 1.8 mm/s and an isomer shift equal to 1.11 mm/s, is taken into account. This signal is attributed to Fe^{2+}. The quadrupole splitting value is slightly smaller than those observed by Dollase and provides no definite site information (Dollase, 1973). According to Dollase (1973), the Fe^{2+} doublet is characterized by $1.89 \leq \Delta \leq 2.28$ and $0.88 \leq \delta \leq 1.07$ mm/s, relative to ^{57}Fe in Pd. However, considering the detection limit of the Mössbauer apparatus (±3% of the signal area), the estimation of Fe^{2+} ion sites in the epidote structure is questionable and, moreover, does not affect significantly the inferred order-disorder relationships noted below.

Substitutional order-disorder in epidotes

From the chemical compositions and the relative amounts of Fe contents attributed to each of the various doublets, Fe^{3+} (and Fe^{2+}) site occupancies have been calculated. The results are given in Table 4. The Fe^{3+} content accommodated in the M1 sites ranges from approximately 0 to 0.09 atom per formula unit. Fe^{3+} ions assigned to the M3 sites ($X_{Fe^{3+},M3}$) represent the majority of the total Fe^{3+} content: $0.58 \leq X_{Fe^{3+},M3} \leq 0.77$ (per formula unit). If it is assumed that a completely ordered epidote contains Fe^{3+} ions only in the M3 sites, the octahedral disordering can be represented by the following reaction:

$$Fe^{3+}\ M3 + Al^{3+}\ M1 \rightleftharpoons Fe^{3+}\ M1 + Al^{3+}\ M3. \quad (1)$$

The octahedral disordering increases from SM43 ($X_{Fe^{3+},M1} \approx 0$) to SM4 ($X_{Fe^{3+},M1} \approx 0.09$) (Table 4). These results are similar to those observed by Bird et al. (1988) for vein epidote from the biotite zone of the Salton Sea geothermal field. The lowest amount of order is observed for the more Fe-rich compositions (SM4; $X_{Fe^{3+},M1} \approx 0.09$); however, epidote from sample SM112 ($X_{Ps} = 0.26$) is better ordered ($X_{Fe^{3+},M1} \approx 0.04$) than epidote from sample SM17 ($X_{Ps} = 0.25$; $X_{Fe^{3+},M1} \approx 0.07$). Thus, the Fe^{3+} content attributed to M1 sites does not appear to strictly depend on the total Fe content.

TABLE 4. Fe distribution in epidote ($X_{Fe^{3+},M1}$, $X_{Fe^{3+}M3}$, $X_{Fe^{2+}}$), and deviation from equilibrium theoretical values ($X_{Fe^{3+}M1}$)

	Samples					
	SM4a	SM4b	SM14	SM17	SM112	SM43
			Mössbauer data			
XFe^{3+}	0.77	0.75	0.75	0.69	0.74	0.58
M3	±0.03	±0.03	±0.03	±0.03	±0.03	±0.02
XFe^{3+}	0.09	0.09	0.07	0.07	0.04	±0.01
M1	±0.03	±0.03	±0.03	±0.03	±0.02	
XFe^{2+}		±0.02				
			Theoretical calculation			
XFe^{3+}	0.85	0.84	0.81	0.76	0.77	0.59
M3	±0.01	±0.01	±0.01	±0.01	±0.01	±0.01
XFe^{3+}	0.01	0.01	±0.005	±0.005	0.01	±0.005
M1	±0.005	±0.005			±0.005	
$\Delta X_{Fe^{3+},M1}$	0.08	0.08	0.065	0.065	0.03	±0.01
	±0.03	±0.03	±0.03	±0.03	±0.02	

Note: For theoretical calculation, (Fe^{3+} + Al^{3+}) value is reduced to 3. Estimated errors are calculated from accuracies of Mössbauer spectroscopy and microprobe.

DISCUSSION

Determination of the nonequilibrium ordering state

The influence of composition on ordering has been demonstrated by Molin (1989) for disordering in orthopyroxenes (especially Fe-Mg disordering). For epidote group minerals, the probability of finding Fe^{3+} in M1 sites increases with the Fe content of epidotes. Dollase (1973) observed that in epidote with Fe^{3+} contents up to 0.8 Fe^{3+} ions per formula unit, the M1 octahedra are nearly free of Fe^{3+}.

The chemical dependence is not clearly established in this study. However, the maximum and minimum values of $X_{Fe^{3+},M1}$ are obtained for the less and more Fe-rich epidote samples respectively, yielding a rough correlation.

The influence of temperature on ordering has also been noted by Molin (1989); disordering in orthopyroxenes also depends on the temperature to which the crystal was heated and the length of time for which it was held at this temperature (for heated and quenched samples). Theoretical curves (Fig. 5) have been calculated to point out the temperature dependence of $X_{Fe^{3+},M1}$ in epidote. These theoretical Fe^{3+} distribution curves have been established by Bird et al. (1988) from Bird and Helgeson's model (1980). In this model, the equilibrium distribution of Fe^{3+} in M3 sites is given by

$$X_{Fe^{3+},M3} = -\{[X_{Ep}(1 - X_{\Sigma,M3})/(K - 1)] + [(K - KX_{Ep} + X_{Ep} + 1 - X_{\Sigma,M3})/2(K - 1)]^2\}^{1/2} - \{[K(1 - X_{Ep}) + X_{Ep} + 1 - X_{\Sigma,M3}]/2(K - 1)\}$$

where K is the intracrystalline standard state equilibrium constant for Reaction #1, $X_{Ep} = X_{Ca_2FeAl_2Si_3O_{12}(OH)}$, and $X_{\Sigma,M3}$ is the sum of the mole fractions of ions other than Fe^{3+} and Al^{3+} in the M3 site. The equilibrium constant K is calculated for each temperature T, using the equation $\log K = -1523.4(1/T - 1/T_r) - 5.0$, where $T_r = 298.15$ K (Bird and Helgeson, 1980). It should be noted that Bird and Helgeson calculated values of K for the intracrystalline exchange assuming ideal mixing of Fe + Al on M1 and M3 sites.

Theoretical $X_{Fe^{3+},M1}$ values have been calculated for our samples. $X_{\Sigma,M3}$ has been neglected considering the low Mn content of epidotes. The values obtained from Mössbauer data do not match the theoretical values and correspond to an equilibrium state of order between 500 and greater than 600 °C. Thus the epidote samples studied are more disordered than epidotes crystallizing in an equilibrium state as predicted by the equations and data of Bird and Helgeson (1980).

In order to compare all of the investigated samples, the deviation from equilibrium state ($\Delta X_{Fe^{3+},M1}$) has been calculated. Values of $\Delta X_{Fe^{3+},M1}$ range from approximately 0 to 0.08. The maximum value is obtained for sample SM4. This parameter has been plotted as a function of temperature (Fig. 6) and can be fit by the equation $T \approx 332 - 1474\Delta X_{Fe^{3+},M1}$ (coefficient for regression = −0.98).

It appears that $\Delta X_{Fe^{3+},M1}$ is closely related to the distribution of paleotemperature. The degree of disorder increases with the distance from the thermal source. Because temperatures vary with time at any point around the intrusion (Norton, 1982), all temperature-dependent parameters (in this case, deviation from equilibrium state) are also time dependent.

Geological interpretation

According to Carpenter and Putnis (1985), it appears, in general, that at conditions of sufficient supersaturation, the disordered phase is kinetically favored over its ordered equivalent. Indeed, if the growth rate is high, there is an increased probability that a wrong atom would be trapped in place by succeeding atoms. Bird et al. (1988), therefore, explain the nonequilibrium ordering state in their samples by possible variations in temperature and in flux and composition of hydrothermal fluids during the evolution of the geothermal system that led to conditions favoring rapid formation of metastable secondary minerals. A previous study of crystal sizes (Patrier et al., 1990) points out a close relation between epidote size and

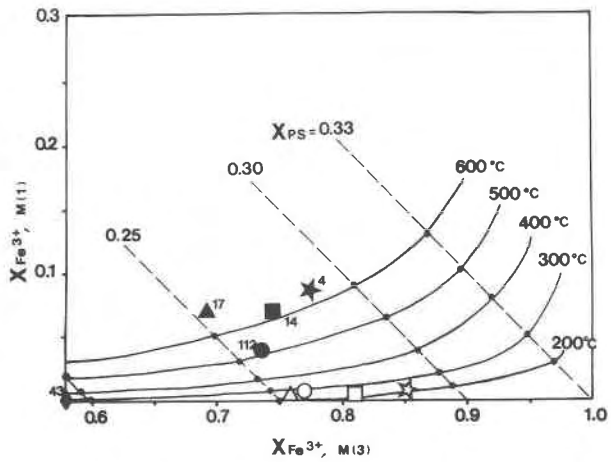

Fig. 5. Theoretical distribution of Fe^{3+} in M1 and M3 sites in epidote, determined by Bird et al. (1988) from Bird and Helgeson (1980). Solid symbols = observed values for the investigated samples; open symbols = theoretical values for the same samples denoted by the solid symbols.

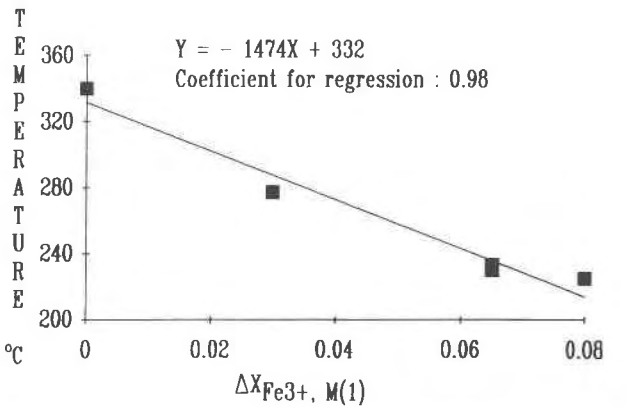

Fig. 6. Deviation from equilibrium theoretical values ($\Delta X_{Fe^{3+},M1}$) as a function of the temperature that affected the samples during epidote crystallization.

paleotemperatures estimated from fluid inclusions in quartz. The results suggest an exponential dependence of crystallization rate (growth and nucleation rate) upon temperature as already described by Carlson (1989). According to these data, epidote from sample SM43 crystallized more rapidly than epidote from the outer part of the geothermal system. So, in the case of Saint Martin, rapid crystallization is not sufficient to explain the metastable state of epidote from samples SM4, SM14, and SM17.

Because the metastable state of epidote probably originates with crystallization, later order-disorder transformations must occur. This process involves atomic migration through the crystal. Diffusion in solids is generally very slow, and in many minerals, temperature has to be maintained for a very long time for equilibrium to be achieved (Putnis and McConnell, 1980). According to the model of Norton (1982), which considers a pluton intruded at a depth of approximately 3.5 km and characterized by an initial temperature of 800 °C, just above the pluton's top, the temperature has already reached 300 °C after 10000 years. A temperature of approximately 200 °C is maintained during the next 80000 years. However, for a sample located at 2 km from the pluton's side, the maximum temperature, close to 200 °C, is attained after 60000 to 90000 years. Therefore, near the thermal source, at the higher temperature, diffusion is rapid enough and is maintained over a sufficiently long period for the equilibrium distribution to be nearly achieved. Further from the intrusion center, the original metastable Fe distribution is nearly preserved because of the lower temperature and corresponding lower diffusion rate. According to Seifert and Virgo (1975), for natural anthophyllite, an equilibrium state for a temperature of 270 °C is achieved after 10^7 years. Thus the maintenance of high temperature over a long time seems to be the major control of order-disorder equilibration. Sample SM112, located near zones of active flow, as suggested by the paleotemperature profile, has suffered sufficiently high temperature to move toward an equilibrium state despite the possible variation in flux and in composition of the hydrothermal fluids.

All of these observations of ordering state in secondary minerals suggest, as pointed out by Carpenter and Putnis (1985), that a purely thermodynamic approach, based on equilibrium diagrams, may lead to inaccurate or simply incorrect results.

Influence of the ordering state on epidote composition

The epidote occurring in the ordered sample SM43 has a chemical zonation that sometimes suggests a miscibility gap between a relatively Fe-poor member (X_{Ps} about 0.15) and Fe-rich member (X_{Ps} about 0.25). This chemical discontinuity has been already described by Hietanen (1974), Holdaway (1965), Raith (1976), and Schreyer and Abraham (1978). However, the compositional break is not present in epidote from all greenschist facies and in geothermal fields. Relationships between the ordering state and a possible miscibility gap have already been pointed out by Carpenter and Putnis (1985). Thus, miscibility gaps in plagioclase appear to be dependent directly on the Al/Si ordering transformations; i.e., in the absence of ordering, there is no effective chemical gap. It may be that the chemical breakdown, between $X_{Ps} = 15$ and $X_{Ps} = 25$ is related to the ordered state of epidote. However, because the zoning is not systematically observed, our results, which constitute a first step in the understanding of such chemical variations, must be verified in other locations, especially in active geothermal fields where similar order-disorder behavior in epidote is observed (Bird et al., 1988).

Conclusion

On the basis of ^{57}Fe Mössbauer spectra of epidote samples from the Saint Martin ancient geothermal field, the

location of Fe^{3+} ions has been determined. In more Fe-rich epidotes ($0.25 \leq X_{Ps} \leq 0.30$), Fe^{3+} is accommodated in the M3 and in minor amounts in the M1 sites. This location has been determined previously from Mössbauer spectra by Dollase (1973).

From our results, it appears that epidote exhibits a metastable ordering state with increasing metastability with distance from the intrusion. Equilibrium ordering is only observed for epidote crystallized at temperatures higher than 300 °C. Near the intrusion, the thermal history favored the ordering process, whereas in the outer part of the geothermal field, the diffusion process is too slow to allow ordering.

It would be interesting to compare the extent of the metastable state found for epidotes from Saint Martin with those from active geothermal systems for which precise ages have been determined. Such comparison should give information on the kinetics of epidote ordering. Epidote could then be used as a petrogenetic indicator. Moreover, the possible influence of ordering on chemical zoning must also be tested in other environments.

Acknowledgments

Financial support for this study was provided by the "Programme interdisciplinaire de recherche sur les sciences pour l'énergie et les matières premières" (PIRSEM).

References cited

Bancroft, G.M., Maddock, A.G., and Burns, R.G. (1967) Applications of the Mössbauer effect to silicate mineralogy—I: Iron silicates of known crystal structure. Geochimica and Cosmochimica Acta, 31, 2219–2246.

Beaufort, D., Westercamp, D., Legendre, O., and Meunier, A. (1990) The fossil hydrothermal system of Saint Martin: (I) Geology and lateral distribution of alterations. Journal of Volcanology and Geothermal Research, 40, 219–243.

Bettison, L.A., and Schiffman, P. (1988) Compositional and structural variations of phyllosilicates from the Point Sal ophiolite, California. American Mineralogist, 73, 62–76.

Bird, D.K., and Helgeson, H.C. (1980) Chemical interaction of aqueous solutions with epidote-feldspar mineral assemblages in geologic systems, I: Thermodynamic analysis of phase relations in the system CaO-FeO-Fe_2O_3-Al_2O_3-SiO_2-H_2O-CO_2. American Journal of Science, 280, 907–941.

Bird, D.K., Schiffman, P., Elders, W.A., Williams, A.E., and McDowell, S.D. (1984) Calc-silicate mineralization in active geothermal systems. Economic Geology, 79, 671–695.

Bird, D.K., Cho, M., Janik, C.J., Liou, J.G., and Caruso, L.J. (1988) Compositional, order/disorder, and stable isotope characteristics of Al-Fe epidote, state 2-14 drill hole, Salton Sea geothermal system. Journal of Geophysical Research, 93-B11, 13, 135–13144.

Carlson, W.D. (1989) The significance of intergranular diffusion to the mechanisms and kinetics of porphyroblast crystallization. Contributions to Mineralogy and Petrology, 103, 1–24.

Carpenter, M.A., and Putnis, A. (1985) Cation order and disorder during crystal growth: Some implications for natural mineral assemblages. in A.B. Thompson and D.C. Rubie, Eds., Metamorphic reactions: Kinetics, texture, and deformation, p. 1–26. Springer-Verlag, New York.

Caruso, L.J., Bird, D.K., Cho, M., and Liou, J.G. (1988) Epidote-bearing veins in the state 2-14 drill hole: Implications for hydrothermal fluid composition. Journal of Geophysical Research, 93-B11, 13, 123–13133.

Cavaretta, G., Gianelli, G., Scandiffio, G., and Tecce, F. (1985) Evolution of the Latera geothermal system II: Metamorphic, hydrothermal mineral assemblages and fluid chemistry. Journal of Volcanology and Geothermal Research, 26, 337–364.

Coey, J.M.D. (1984) Mössbauer spectroscopy of silicate minerals. In G.J. Long, Ed., Mössbauer spectroscopy applied to inorganic chemistry, p. 443–509. Plenum Press, New York.

De Coster, M., Pollak, H., and Amelinckx, S. (1963) A study of Mössbauer absorption in iron silicates. Physica Status Solidi, 3, 283–288.

Deer, W.A., Howie, R.A., and Zussmann, J. (1962) Rock-forming minerals, vol. 1. Wiley, New York.

Dollase, W.A. (1971) Refinement of the crystal structures of epidote, allanite and hancockite. American Mineralogist, 56, 447–464.

——— (1973) Mössbauer spectra and iron distribution in the epidote-group minerals. Zeitschrift für Kristallographie, 138, 41–63.

Grapes, R., and Watanabe, T. (1984) Al-Fe^{3+} and Ca-Sr^{2+} epidotes in metagreywacke-quartzofeldspathic schist, Southern Alps, New Zealand. American Mineralogist, 69, 490–498.

Hietanen, A. (1974) Amphibole pairs, epidote minerals, chlorite and plagioclase in metamorphic rocks, Northern Sierra Nevada, California. American Mineralogist, 59, 22–40.

Holdaway, M.J. (1965) Basic regional metamorphic rocks in part of the Klamath Mountains, Northern California. American Mineralogist, 50, 953–977.

Liou, J.G. (1973) Synthesis and stability relations of epidote $Ca_2Al_2FeSi_3O_{12}(OH)$. Journal of Petrology, 14, 381–413.

Miyashiro, A., and Seki, Y. (1958) Enlargement of the composition field of epidote and piemontite with rising temperature. American Journal of Science, 256, 423–430.

Molin, G.M. (1989) Crystal-chemical study of cation disordering in Al-rich and Al-poor orthopyroxenes from spinel lherzolite xenoliths. American Mineralogist, 74, 593–598.

Norton, D.L. (1982) Fluid and heat transport phenomena typical of copper-bearing pluton environments. In S.R. Titley, Ed., Advances in geology of the porphyry copper deposits, Southwestern North America, p. 59–72. The University of Arizona Press, Tucson, Arizona.

Paesano, A., Kunrath, J.I., and Vasquez, A. (1983) A ^{57}Fe Mössbauer study of epidote. Hyperfine Interactions, 15–16, 841–844.

Patrier, P., Beaufort, D., Touchard, G., and Fouillac, A.M. (1990) Crystal size of epidotes: A potentially exploitable geothermometer in geothermal fields? Geology, 18, 1126–1129.

Putnis, A., and McConnell, J.D.C. (1980) Principles of mineral behaviour. In A. Hallam, Ed., 257 p. Blackwell Scientific Publications, Oxford, United Kingdom.

Raith, M. (1976) The Al-Fe(III) epidote miscibility gap in a metamorphic profile through the Penninic series of the Tauern Window, Austria. Contributions to Mineralogy and Petrology, 57, 99–117.

Schreyer, W., and Abraham, K. (1978) Prehnite/chlorite and actinolite/epidote bearing mineral assemblages in the metamorphic igneous rocks of La Helle and Challes, Venn-Stavelot-Massif, Belgium. Annales de la Société Géologique de Belgique, 101, 227–241.

Seifert, F.A., and Virgo, D. (1975) Kinetics of the Fe^{2+}-Mg, order-disorder reaction in anthophyllites: Quantitative cooling rates. Science, 188, 1107–1109.

Shikazono, N. (1984) Compositional variations in epidote from geothermal areas. Geochemical Journal, 18, 181–187.

Manuscript received December 4, 1989
Manuscript accepted December 21, 1990